YMTHE, Volume *27*

Supplemental Information

Engineering of a Lectibody Targeting High-Mannose-Type Glycans of the HIV Envelope

Krystal Teasley Hamorsky, J. Calvin Kouokam, Matthew W. Dent, Tiffany N. Grooms, Adam S. Husk, Steven D. Hume, Kenneth A. Rogers, Francois Villinger, Mary Kate Morris, Carl V. Hanson, and Nobuyuki Matoba

1. Supplementary Figures

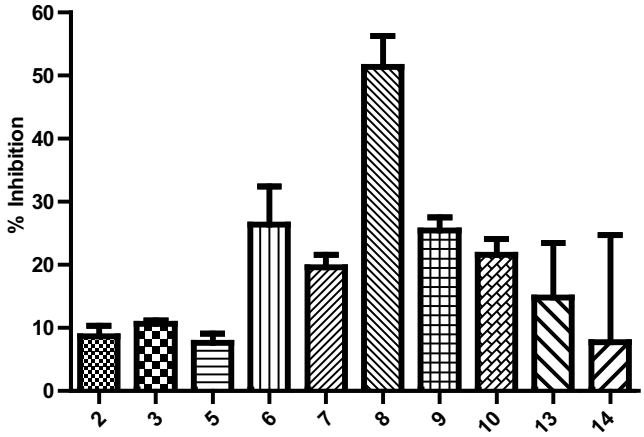

Figure S1. Analysis of the anti-HIV activity of AH variants in crude leaf extracts. A syncytium formation assay was utilized to assess the anti-HIV activity of crude leaf extracts from plants expressing AH variants that showed a positive signal in gp120-ELISA in Fig. 1c (i.e., Variants 2, 3, 5, 6, 7, 8, 9, 10, 13 and 14). A 1/20 final dilution of extract was mixed with HL2/3 cells expressing HIV gp120 and TZM-bl $CD4^+$ cells and incubated for 18 h. % Inhibition was reflected by the reduction in β-galactosidase activity based on HL2/3 plus TZM-bl cells only control. Variant 8, named Avaren, was determined to be the best variant.

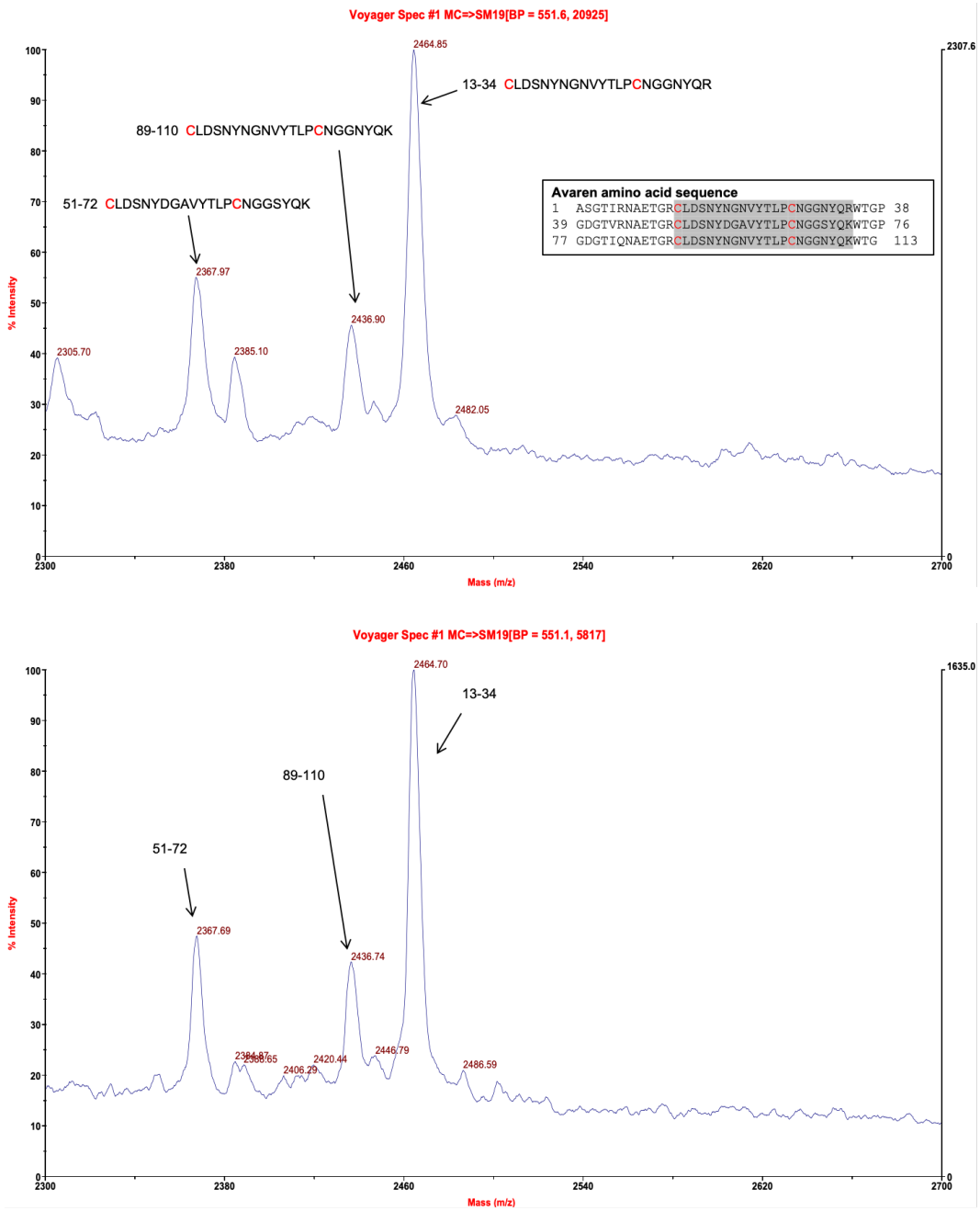

Figure S2. Matrix Assisted Laser Desorption Ionization Time-of-flight Mass Spectrometry (MALDI-TOF MS) analysis of Avaren. Purified Avaren was first digested with trypsin. Before MALDI-TOF analysis, the half of the tryptic digest was reduced with DTT and alkylated with iodoacetamide (top panel), and the other half was alkylated only without reduction (bottom panel). The presence of the three peptides (corresponding to the grey sequences of Avaren in the box) in the top panel provides evidence that the two Cys in each peptide are not bound to Cys in a different peptide. Additionally, alkylation without reduction shows the same three peptides in the bottom panel, suggesting that the Cys residues are not free but part of a disulfide bond within each peptide. The analysis was performed at Columbia University Protein Core Facility.

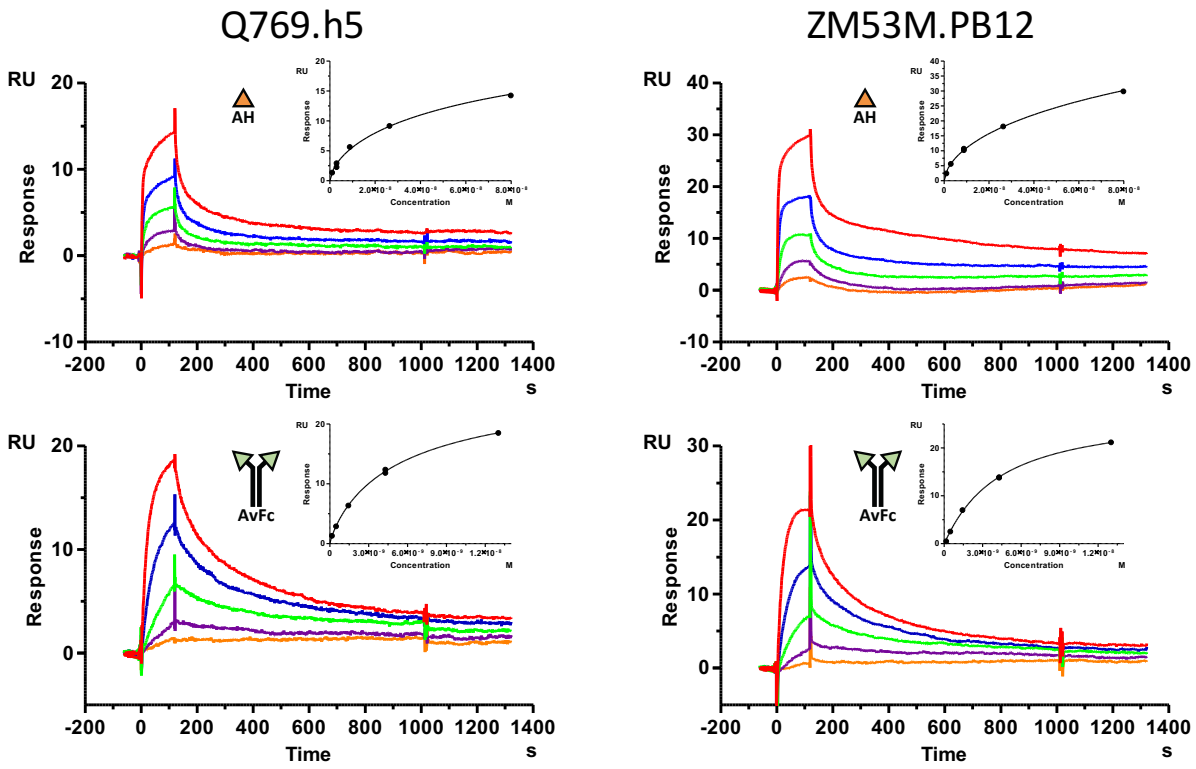

Figure S3. Surface plasmon resonance analysis of the binding affinities of AH and AvFc to gp120 proteins. The binding affinities (K_D) of AH (top) and AvFc (bottom) to $gp120_{(Q769.h5 \text{ or } ZM53M.PB12)}$ were measured using a Biacore X100 2.0 instrument at ambient temperature. For each protein, the assay was performed in duplicate. Representative sensorgrams are shown. Recombinant His-tagged gp120 (from Q769.h5 or ZM53M.PB12 strains) was captured on a sensor chip NTA following the manufacture's instructions to a surface density of about 50-100 RU. Three fold serial dilutions of AvFc (1 µg/ml to 0.0123 µg/ml) or AH (1 µg/ml to 0.0123 µg/ml) were made in running buffer (HPS-P+ with 50 µM EDTA) and injected, at a flow rate of 5 µl/min. The equilibrium dissociation constant K_D was determined based on steady state (inset). The K_D values for AH and AvFc to $gp120_{Q769.h5}$ were determined to be 29.6 ± 1.4 nM and 4.2 ± 0.6 nM, respectively. The K_D values for AH and AvFc to $gp120_{ZM53M.PB12}$ were determined to be 35.7 ± 0.1 nM and 4.4 ± 0.2 nM, respectively. Data are mean ± SEM from two independent analyses.

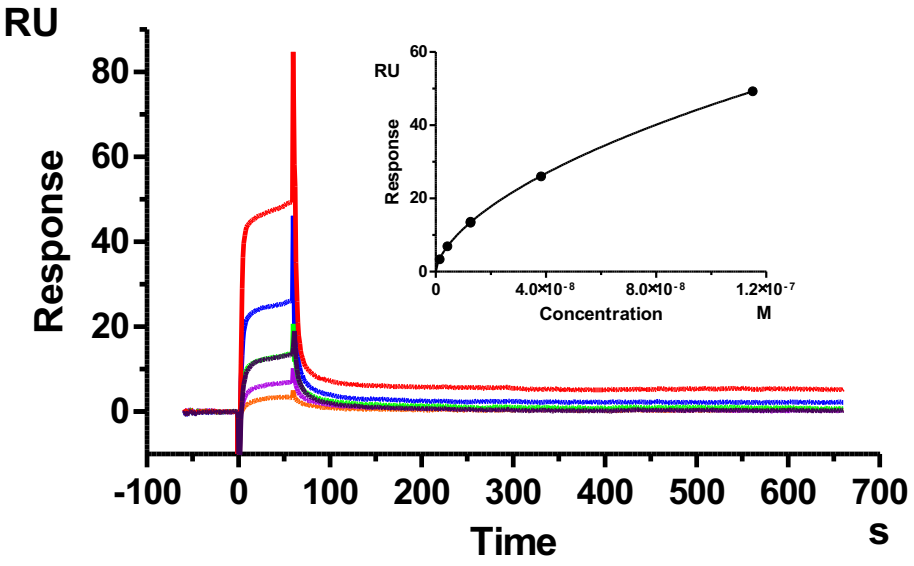

Figure S4. Surface plasmon resonance analysis of AvFc's binding to FcRn. The binding affinity (K_D) of AvFc to FcRn was measured using a Biacore X100 2.0 instrument at ambient temperature. AvFc was captured on a $gp120_{CM}$ immobilized CM5 chip to a surface density of about 120 RUs. Three fold serial dilutions of recombinant human FcRn (5 µg/ml to 0.0617 µg/ml) were prepared in running buffer (HPS-P+) and injected, at a flow rate of 5 µl/min. The equilibrium dissociation constant, K_D, was determined to be 60.1 ± 2.2 nM based on steady state (inset). Data are mean ± SEM of two independent analyses, and a representative sensorgram is shown.

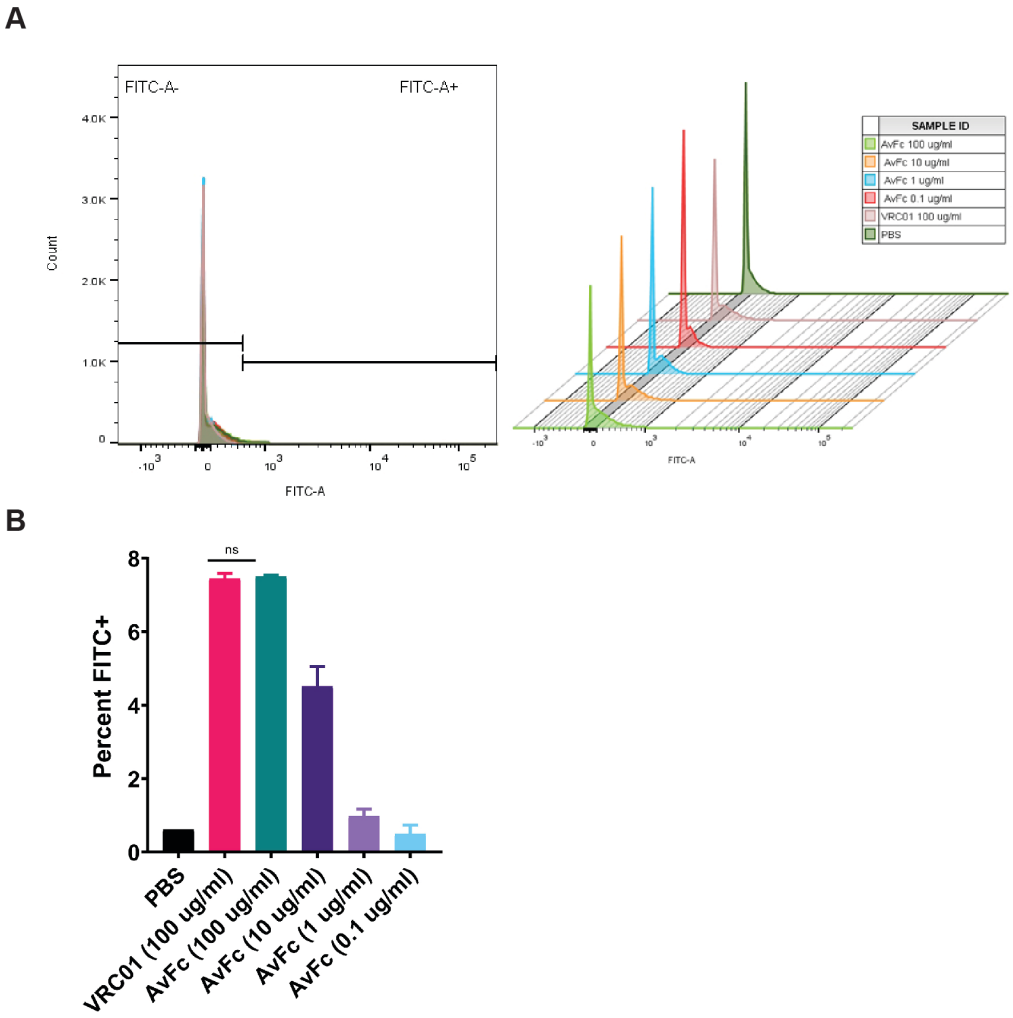

Figure S5. Binding analysis of AvFc to human PBMCs. Binding of AvFc to human PBMCs was evaluated by flow cytometry with a single color (FITC) stain. Multiple concentrations of AvFc (four 1:10 dilutions beginning at 100 µg/mL) were compared to a human IgG (VRC01). **(A)** FITC+ and FITC- populations were gated based on the background fluorescence of unstained PBMCs. **(B)** Quantification of the percentage of total cells that were FITC+. A dose dependent increase in binding to PBMCs occurs with AvFc, however at 100 µg/mL VRC01 bound similarly, indicating that the interaction is not through the Avaren domain. Groups were compared using one-way ANOVA ($p < 0.0001$), and multiple comparisons were corrected for using Tukey's method. The mean percentages of the VRC01 and AvFc 100 µg/mL groups were not statistically different.

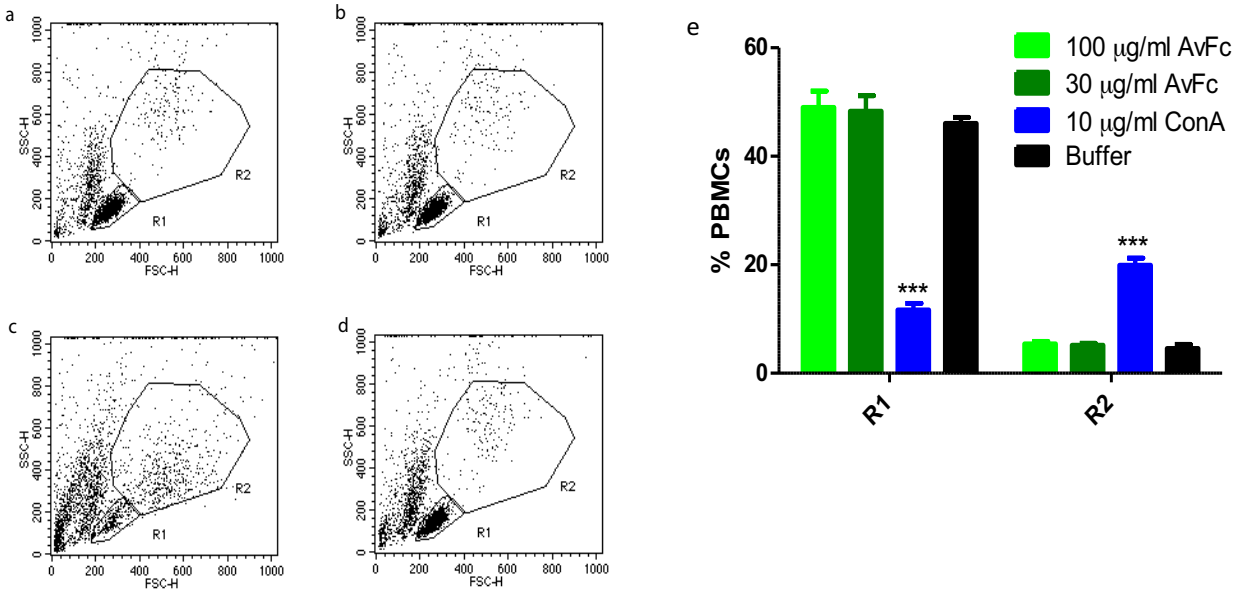

Figure S6. Mitogenic activity of AvFc on PBMC as evaluated by flow-cytometry. Cell were treated with 100 μg/ml AvFc (a), 30 μg/ml AvFc (b), 10 μg/ml ConA (c), and buffer (d) for three days, and analyzed flow-cytometrically. Typical live PBMC were gated in region R1, and a subpopulation with increased size and higher SSC was gated in region R2. Quantitation of cells in these regions is shown in e. ***$P < 0.001$; one-way ANOVA with Bonferroni's posttests. Data are mean ± SD of triplicate experiments, performed in a total of three PBMC preparations.

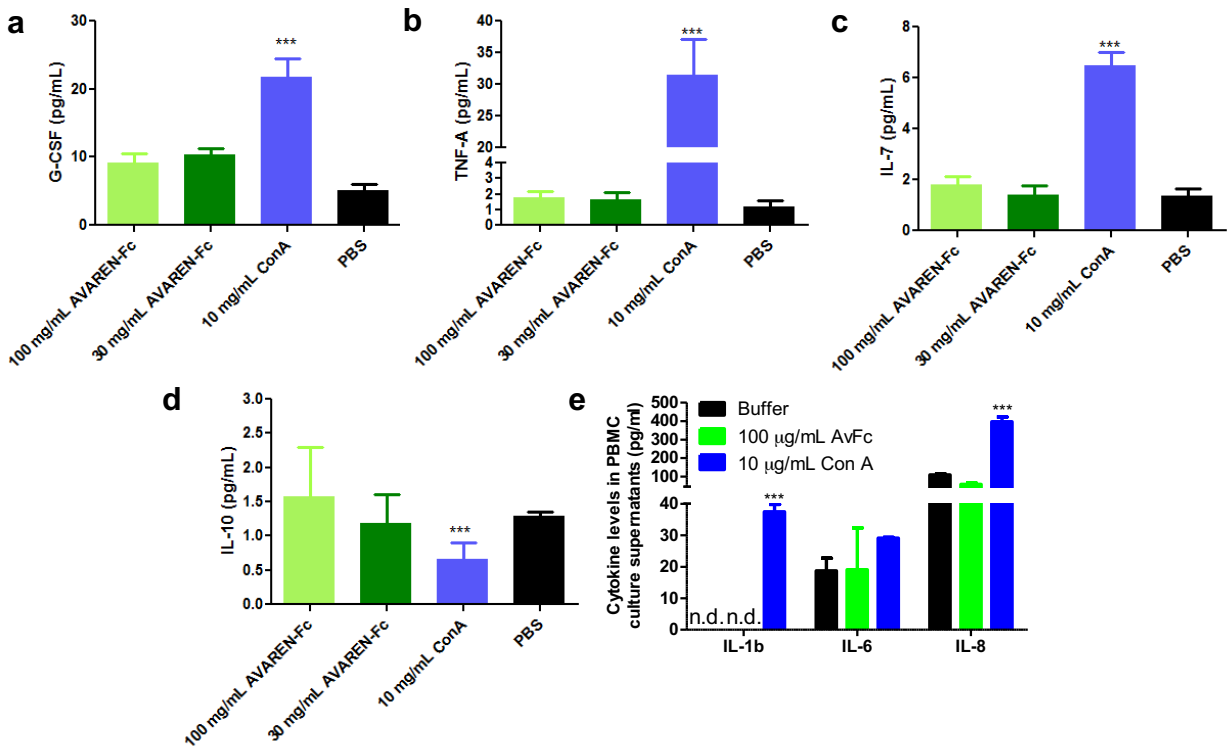

Figure S7. The amounts of inflammatory mediators that appeared to be stimulated by AvFc in a multiplex bead array analysis. G-CSF (a), TNF-α (b), IL-7 (c), and IL-10 (d)levels were increased in some PBMC specimens, when cells were treated with AvFc at 100 μg/ml. However, no statistical significance was obtained for their absolute levels when PBMC samples from all donors were considered. ***$P < 0.001$; one-way ANOVA with Bonferroni's posttests. e. Confirmation of the multiplex bead array results by individual cytokine ELISA. Treatment of PBMCs with 100 μg/ml AvFc resulted in IL-1b, IL-6, and IL-8 levels similar to those obtained with the buffer. n.d. (levels below detection). ***$P < 0.001$; one-way ANOVA with Bonferroni's posttests. Data are mean ± SD of triplicate experiments, performed in a total of three PBMC preparations.

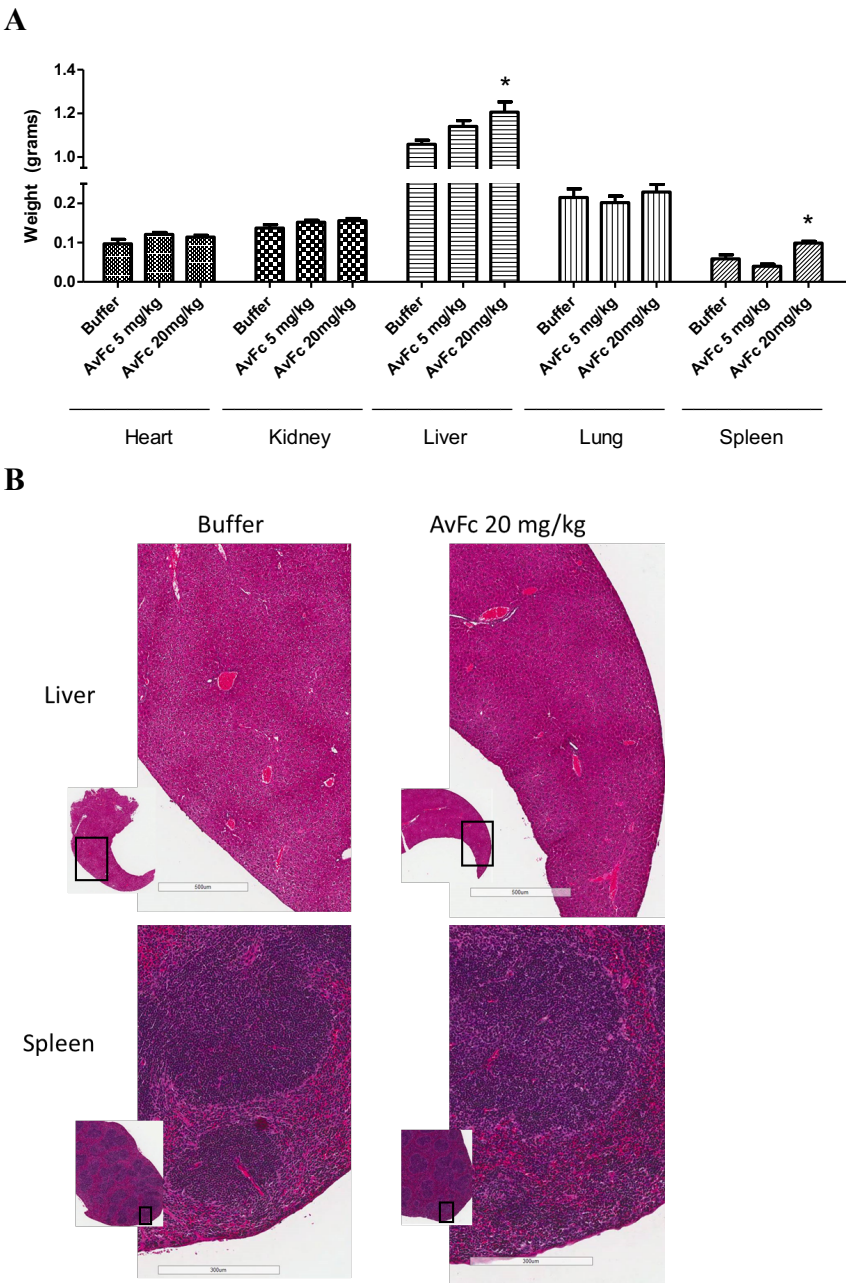

Figure S8. Effect of AvFc treatment on mouse organ weights and histology, complete blood count and serum chemistry. To evaluate effects of a single high dose of AvFc, mice were injected subcutaneously with buffer (n = 10), 5 mg/kg AvFc (n = 10) or 20 mg/kg AvFc (n = 10) twice a week for 5 weeks. Animals were sacrificed on day 35 and blood was taken from the inferior vena cava of each animal for complete blood count and serum chemistry analysis (See Tables S2 and S3). Organs were excised, weighed, fixed in 10% buffered formalin for 16 h, and stored in 70% ethanol until paraffin embedding, sectioning, and routine hematoxylin and eosin staining. (A) Major organ weights of buffer control, 5 mg/kg AvFc and 20 mg/kg AvFc groups (mean ± SEM). *$P < 0.05$; one-way ANOVA with Bonferroni's posttests. (B) Representative photographs showing hematoxylin and eosin-stained liver and spleen tissue sections from buffer and 20 mg/kg AvFc groups.

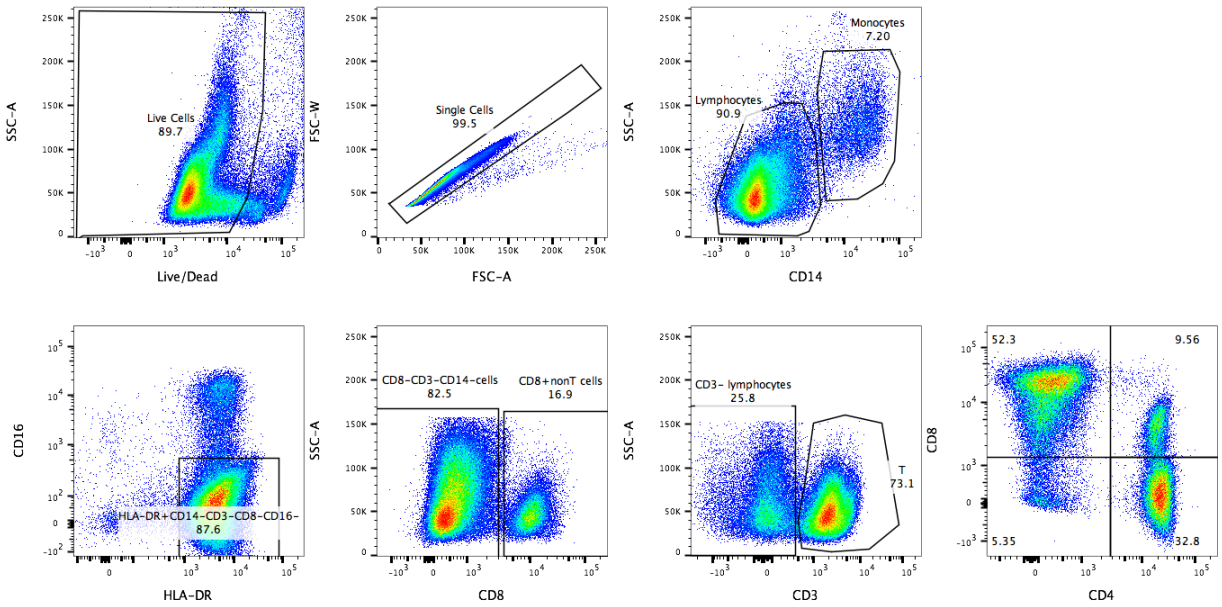

Figure S9. Gating for the analysis of the rhesus macaque PBMCs for the AvFc pharmacokinetic testing. Gates were sequentially drawn for viable cells and singlets, followed by separation of lymphocytes from monocytes. Lymphocytes were subdivided between T cell (CD3+) and non-T cell populations. The T cells were then parsed further using CD4 and CD8. The non-T cell population then had the CD8 population removed, which was analyzed for natural killer (NK) cells, and the CD8- cells then gated for HLA-DR+/CD16- cells to further analysis for dendritic cells (DC).

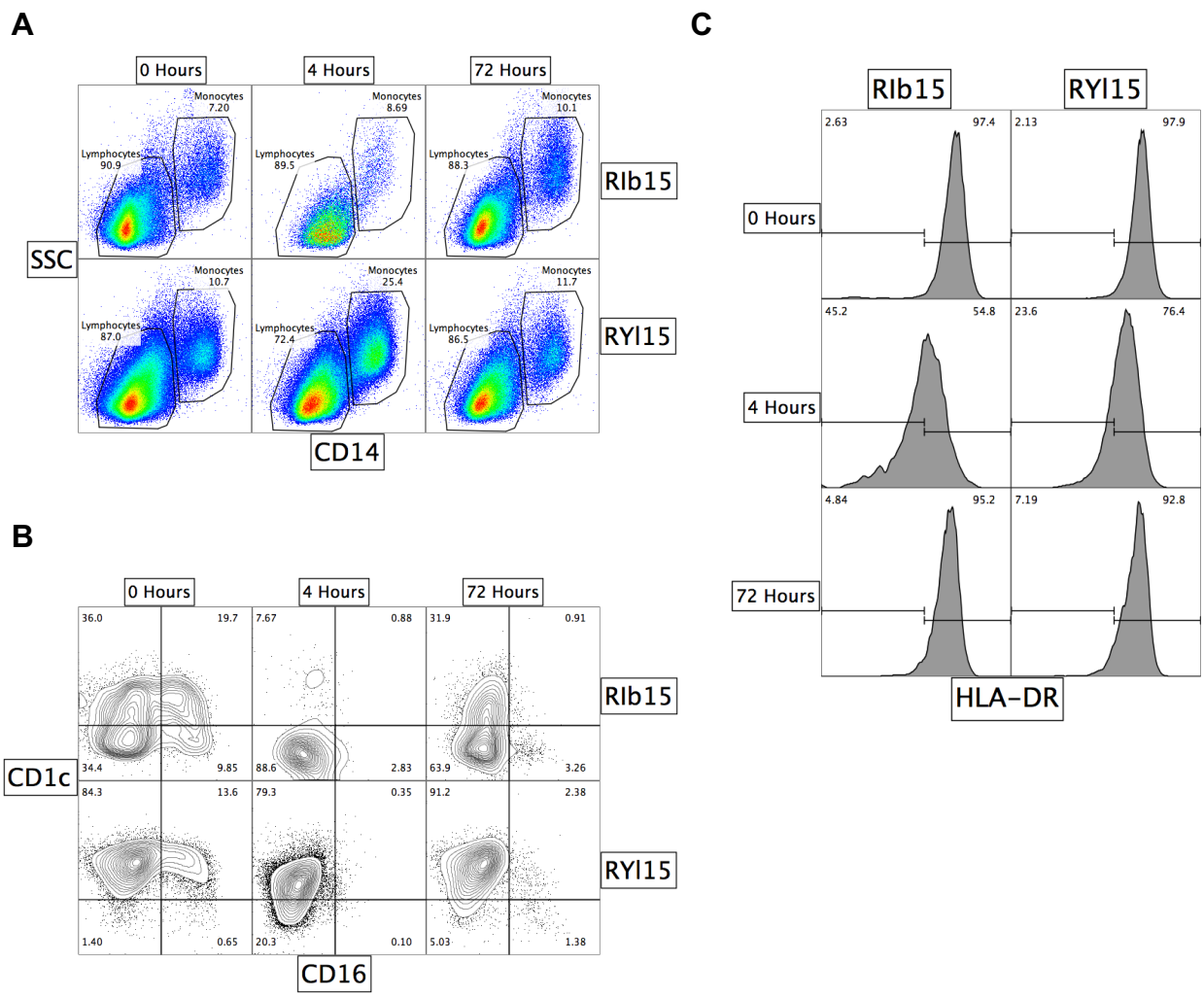

Figure S10. Circulating monocytes following AvFc dosing. (A) CD14+ monocytes increased modestly as a percentage of PBMC 4 h following administration of AvFc and then returned to near baseline value by 72 h. (B) Within this monocyte population, there was a decrease in the percent CD16+ and CD1c+ cells at 4 h, and a rebound of CD1c expression at 72 h, but not CD16. (C) There was also a decrease in the expression of HLA-DR at 4 h post AvFc that rebounded by 72 h.

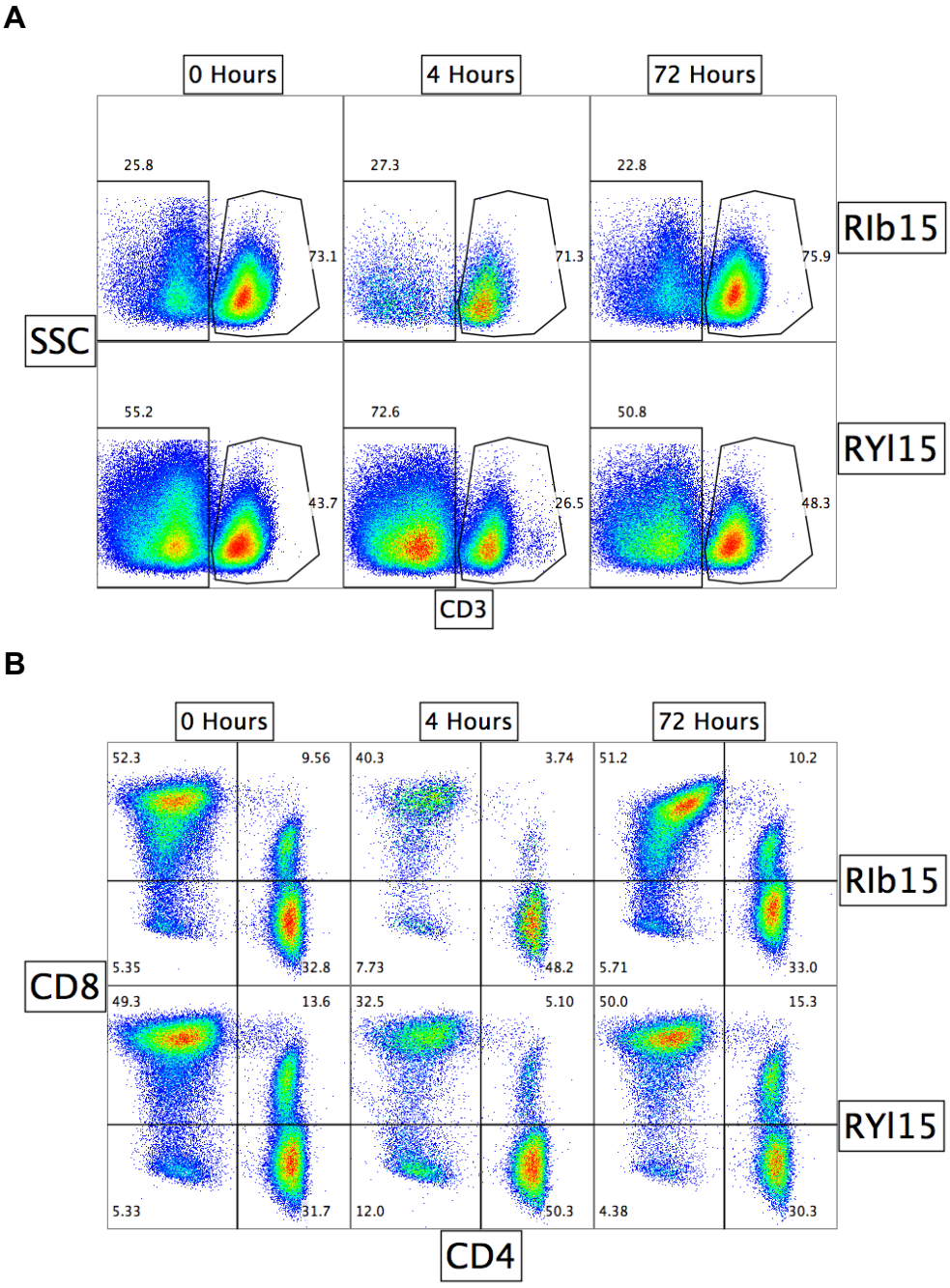

Figure S11. Distribution of T cells following AvFc dosing. (A) T cells (CD3+) as a percentage of lymphocytes remained steady for one animal (RIb15) and decrease at 4 h for the other (RYl15), which was at baseline levels by 72 h. (B) For both animals the ratio of CD8 to CD4 T cells decrease at 4 h and returned to baseline values at 72 h. This change occurred with a drop in the percentage of CD8+CD4- and CD8+CD4+ cells.

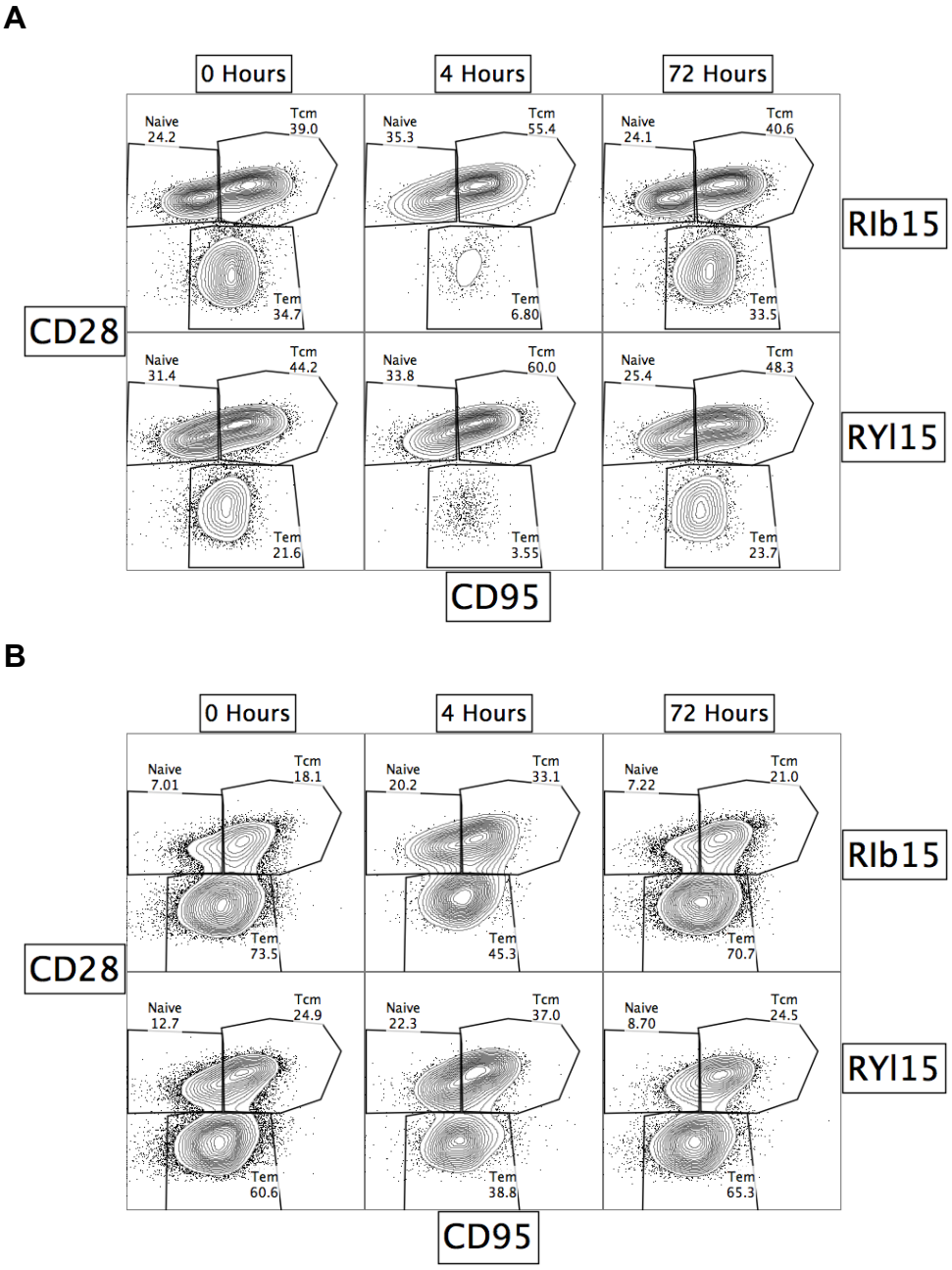

Figure S12. Distribution of T cell subsets following AvFc dosing. (A) T helper cells (CD4+) and (B) Cytotoxic T lymphocytes (CD8+). After dosing AvFc to rhesus macaques, the percentage of effector memory T cells (Tem) decreased at 4 h and rebound at 72 h, indicating the possible short-term trafficking of these cells from the blood to the tissues. Tcm: central memory T cells.

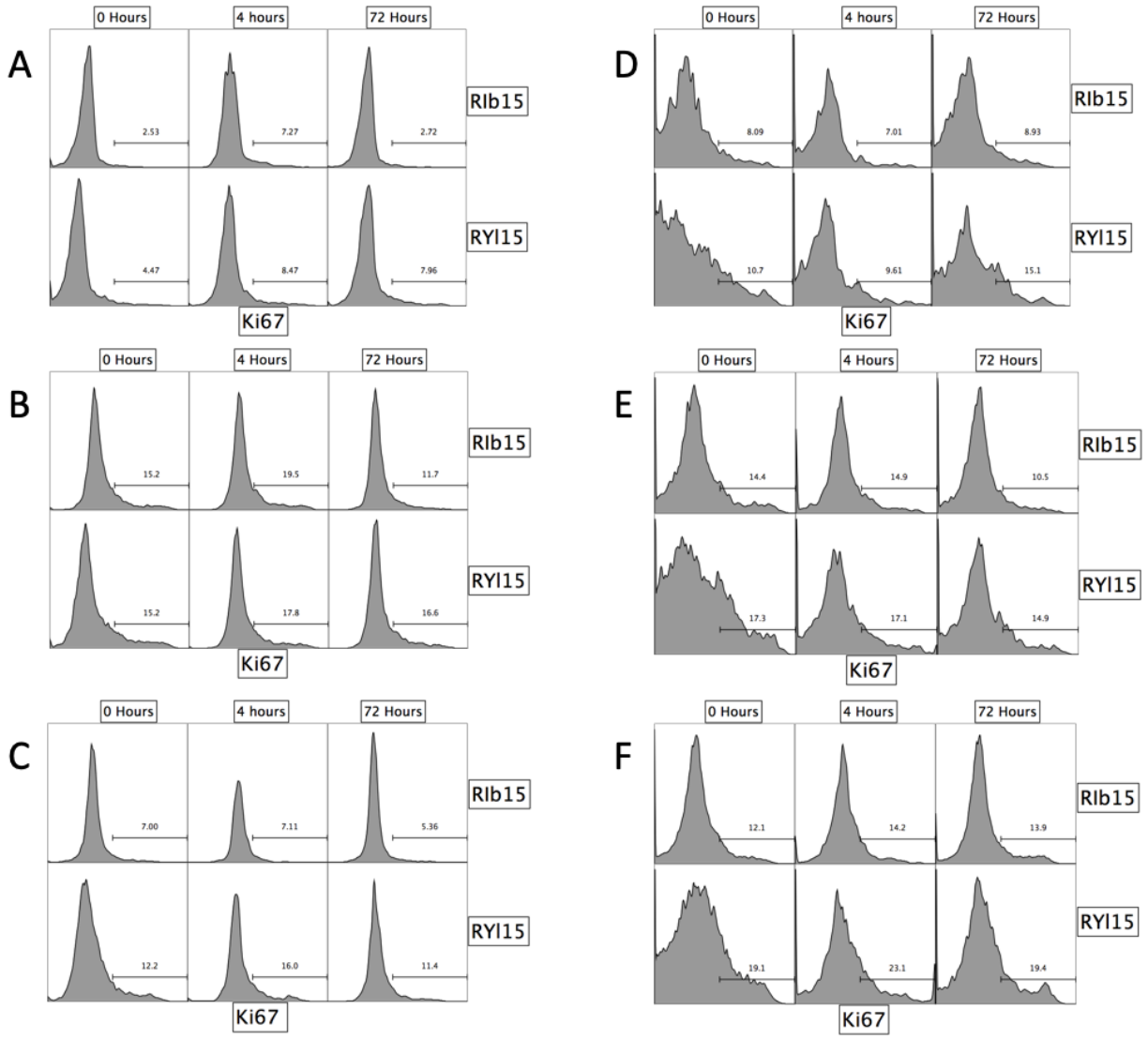

Figure S13. Activation status of T cell subsets following AvFc dosing. (A-C): CD4+ T cells; (D-F): CD8+ T cells. (A and D): naïve T cells; (B and F): Tcm cells; (C and F): Tem cells. Assessment of PBMC T cells activation in rhesus macaques receiving AvFc was done by looking for up regulation of Ki67. Overall there was not up regulation of Ki67 expression in T cells although some modest variation was observed across T cell subsets. See also Figure S14.

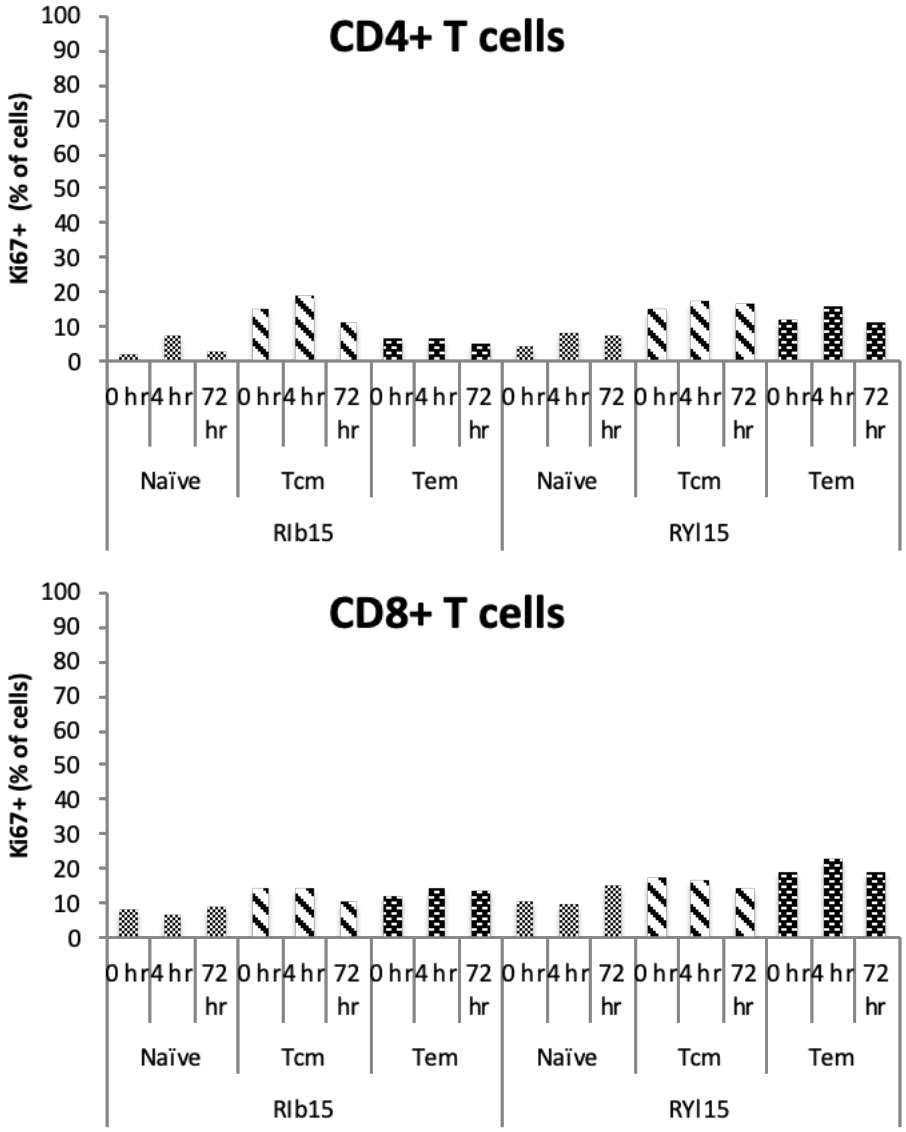

Figure S14. Activation status of T cell subsets following AvFc dosing. Data from Figure S13 are shown as bar graphs for CD4+ and CD8+ T cells.

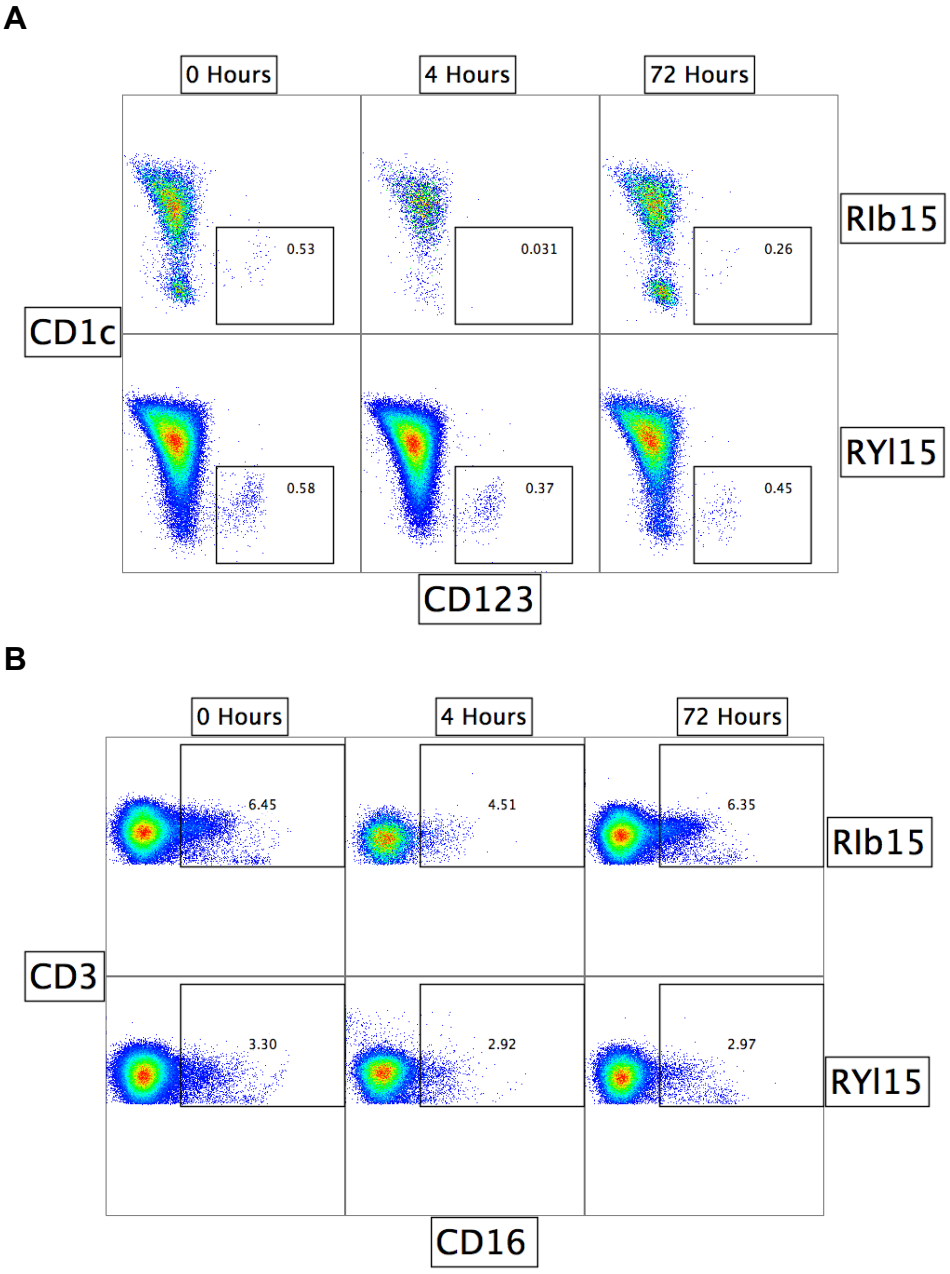

Figure S15. Plasmacytoid dendritic cell (pDC) and NKT cell populations following AvFc dosing. (A) The small population of pDCs (HLA-DR+ CD14-CD3-CD8-CD16- CD123+) decreased as a percent of cells in the blood following administration of AVFc in both rhesus macaques at 4 h and partial rebound by 72 h. (B) Similarly there was a slight decrease in NKT cells CD3+CD16+ as a percentage of total CD3+ cells at 4 h.

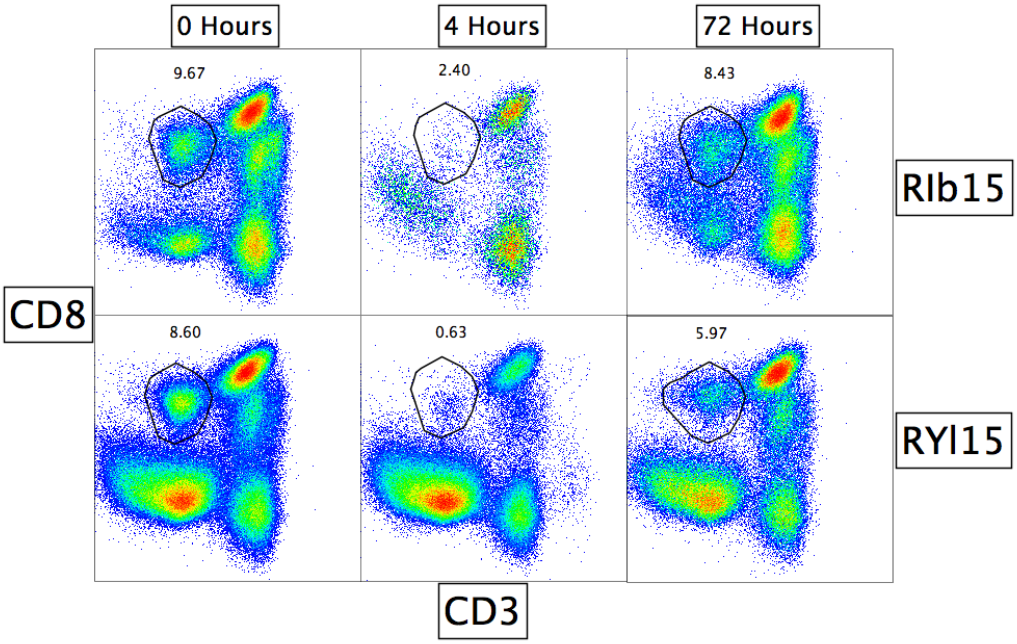

Figure S16. Circulating NK cells following AvFc dosing. A significant population of NK cells (CD8+CD3- lymphocytes) disappeared from the blood 4 h after AvFc administration, but by 72 h they have nearly returned to the baseline level. When NK cells are assessed by gating CD16+ lymphocytes the same results are observed (data not shown).

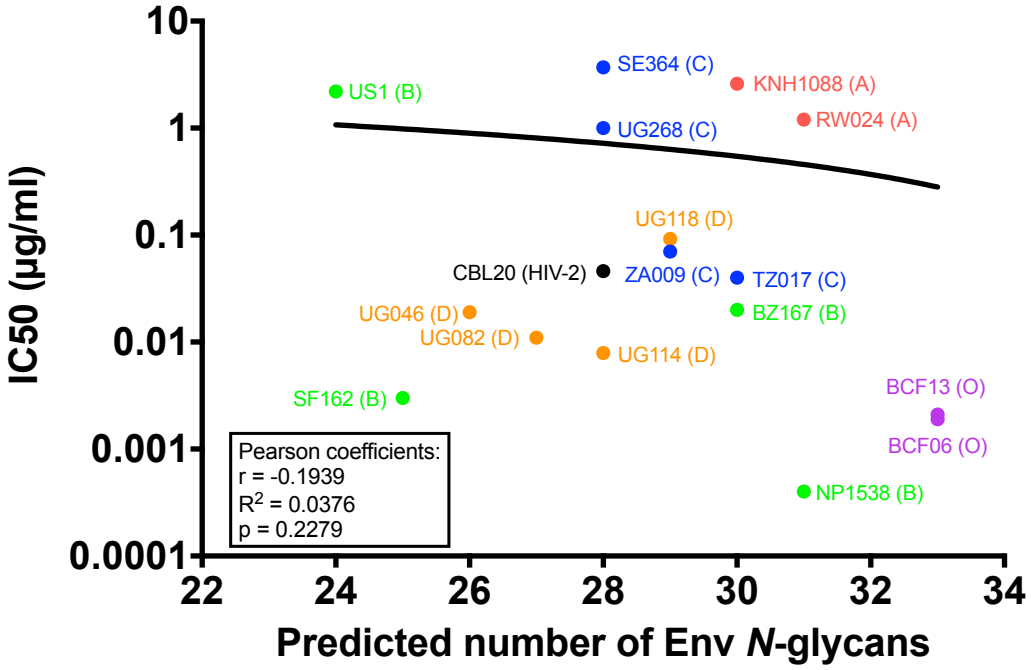

Figure S17. Correlation between the number of Env *N*-glycosylation sites and AvFc IC_{50}s in PBMC-based anti-HIV assay. For primary viruses tested in the PBMC-based anti-HIV assay (Figure 3E), the number of Env *N*-glycosylation sites was plotted against the IC_{50}. *N*-Glycosylation sites were predicted using the NetNGlyc 1.0 Server tool based on the Env amino acid sequence of each virus (US1: AY173952; SE364: L22944; UG268: L22948; KNH1088: AF457063; RW024: AY669699; UG118: AY669751; CBL20: AYA94964.1; ZA009: AY118166; TZ017: AF286235; BZ167: AB485641; UG046: AY669757; UG082: AY669750; UG114: AY494966; SF162: AY669736; NP1538: AY713408; BCF13: KU168291; BCF06: AB485666). The Correlation was analyzed by the Pearson's correlation coefficient (GraphPad Prism). The correlation coefficient (r, R^2) and p values are shown in the graph. Linear regression analysis was used to display a best fit line to the data.

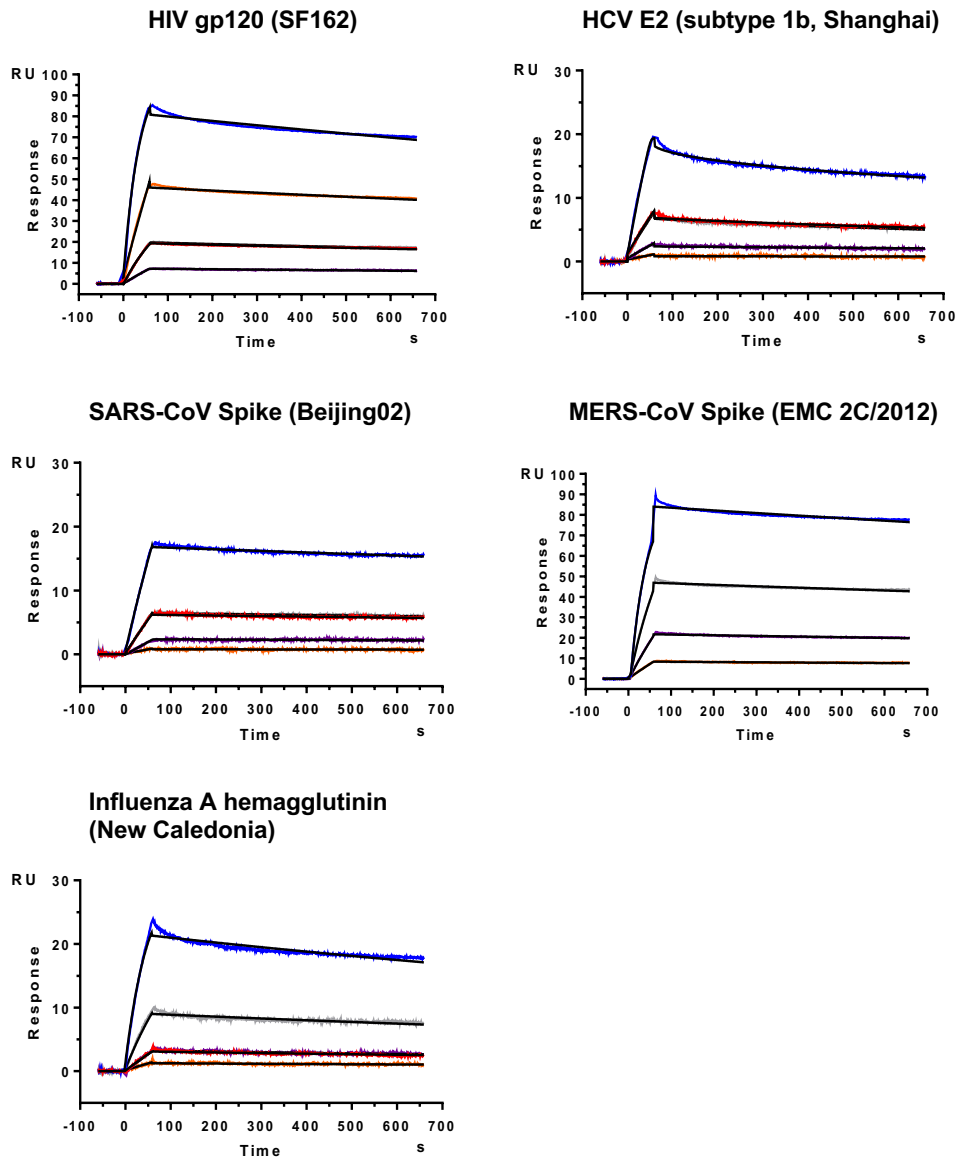

Figure S18. Surface plasmon resonance analysis of AvFc's affinity to viral glycoproteins. The binding affinity (K_D) of recombinant proteins to AvFc was measured using a Biacore X100 2.0 instrument at ambient temperature. AvFc was captured on a sensor chip via an anti-human IgG (Fc) antibody of IgG1 isotype to a surface density of about 300 RU and varying concentrations of recombinant proteins were used as the analytes. Recombinant glycoproteins (HIV SF162, hepatitis C virus [HCV] E2, severe acute respiratory syndrome-coronavirus [SARS-CoV, Beijing02], Middle East respiratory syndrome coronavirus various [MERS-CoV, EMC 2C/2012] and influenza A [New Caledonia] hemagglutinin) were purchased from Immune Technology Corp. (New York, NY). A representative sensorgram for each glycoprotein is shown. The raw curves (colored lines) and the fitted curves (black lines) represent the concentration of recombinant analyte. The equilibrium dissociation constants, K_D, was determined to be based on the 1:1 binding kinetics after airspikes and reference subtracted spikes were removed. K_D and Chi^2 values are shown in **Table S4**.

2. Supplementary Tables

Table S1. Relative expression of selected cytokine and chemokine genes in human PMBCs after treatment with AvFc (100 and 30 µg/ml) and 10 µg/ml ConA as evaluated by quantitative PCR.

	100 µg/ml AvFc	30 µg/ml AvFc	10 µg/ml ConA
	Means ± SEM (n = 3)	Means ± SEM (n = 3)	Means ± SEM (n = 3)
CCL2	1.47 ± 0.26	1.60 ± 0.52	7.44 ± 3.25
CCL3	0.72 ± 0.10	0.72 ± 0.09	1.60 ± 1.06
CCL5	0.96 ± 0.13	1.05 ± 0.04	0.99 ± 0.31
CSF2	0.89 ± 0.77	1.14 ± 0.88	1778.30 ± 1380.19
CSF3	0.23 ± 0.15	0.89 ± 1.19	19.04 ± 23.32
CXCL10	8.90 ± 8.54	5.95 ± 4.66	142.13 ± 156.96
IFN-G	7.64 ± 10.33	13.16 ± 18.33	10815.00 ± 11127.79
IL-10	1.23 ± 0.65	1.13 ± 0.11	6.52 ± 1.94
IL-12A	0.85 ± 0.16	0.96 ± 0.11	1.70 ± 0.45
IL-13	n.d.	n.d.	1722.49*
IL-15	1.31 ± 0.52	1.25 ± 0.26	3.89 ± 0.96
IL-1A	0.90 ± 0.46	0.92 ± 0.16	74.32 ± 79.71
IL-1B	0.89 ± 0.56	1.06 ± 0.26	135.35 ± 109.88
IL-2	1.48 ± 1.29	1.39 ± 0.76	1062.75 ± 645.83
IL-3	1.41 ± 0.69	1.03*	2289.12 ± 828.93
IL-4	n.d.	n.d.	536.48 ± 620.80
IL-5	n.d.	n.d.	562.94 ± 597.96
IL-6	1.53 ± 0.54	1.62 ± 1.21	518.55 ± 443.20
IL-7	1.49 ± 0.30	1.40 ± 0.22	2.54 ± 0.53
IL-8	1.97 ± 0.93	1.43 ± 0.37	71.93 ± 60.94
TNF-A	1.35 ± 0.36	1.24 ± 0.47	26.54 ± 7.66

n.d.: non detected. *: Detected only in one PBMC sample.

Table S2. Serum chemistry profiles of mice following repeated AvFc administration.

Parameter	Unit	Buffer	AvFc 5mg/kg	AvFc 20mg/kg
ALB	g/dL	1.3 ± 1.1	1.8 ± 0.8	2.3 ± 1.1
ALKP	U/L	230.7 ± 136.2	209.5 ± 51.8	243.5 ± 85.74
ALT	U/L	339.8 ± 315.7	160.9 ± 78.1	156.8 ± 51.1
AMYL	U/L	1604.0 ± 998.9	1271.0 ± 522.6	1517.0 ± 552.3
BUN	mg/dL	32.0 ± 5.3	26.0 ± 5.1*	25.6 ± 4.6*
Ca	mg/dL	18.0 ± 3.3	13.87 ± 2.5*	14.3 ± 3.1*
CHOL	mg/dL	51.3 ± 58.4	48.3 ± 39.6	43.7 ± 41.6
CREA	mg/dL	1.4 ± 1.5	0.8 ± 1.2	0.5 ± 0.3
GLOB	g/dL	2.2 ± 1.8	2.5 ± 1.2	2.5 ± 1.1
GLU	mg/dL	299.0 ± 123.3	270.6 ± 58.52	265.3 ± 88.0
PHOS	mg/dL	14.6 ± 3.1	12.3 ± 2.6	12.0 ± 2.4
TBIL	mg/dL	0.8 ± 0.6	0.5 ± 0.4	0.4 ± 0.1
TP	g/Dl	3.6 ± 3.0	4.4 ± 1.8	4.8 ± 1.3

Data represent mean ± SEM. *$P < 0.05$; one-way ANOVA with Bonferonni's posttests compared to the Buffer control. See also Figure 5H in the manuscript.

Table S3. Hematological profiles of mice following repeated AvFc administration.

Cell Type	Parameter	Unit	Buffer	AvFc 5mg/kg	AvFc 20mg/kg
Leukocyte	WBC	k/µL	8.6 ± 1.8	7.1 ± 1.7	7.6 ± 2.6
	NE	k/µL	2.2 ± 0.7	2.1 ± 0.9	2.4 ± 0.8
	LY	k/µL	5.0 ± 0.8	4.0 ± 0.7	4.1 ± 1.5
	MO	k/µL	0.9 ± 0.4	0.7 ± 0.3	0.8 ± 0.3
	EO	k/µL	0.3 ± 0.4	0.2 ± 0.2	0.3 ± 0.2
	BA	k/µL	0.1 ± 0.1	0.1 ± 0.1	0.1 ± 0.1
Erythrocyte	RBC	M/µL	11.7 ± 1.3	10.7 ± 1.0	11.6 ± 1.7
	Hb	g/gL	17.6 ± 2.0	16.3 ± 1.2	17.6 ± 1.5
	HCT	%	62.6 ± 6.8	57.3 ± 5.7	60.1 ± 6.4
	MCV	fL	53.7 ± 1.3	53.7 ± 1.1	53.2 ± 1.2
	MCH	Pg	15.1 ± 0.3	15.3 ± 0.5	15.6 ± 0.8
	MCHC	g/dL	28.1 ± 0.9	28.6 ± 1.4	29.4 ± 2.0
	RDW	%	17.1 ± 0.7	16.9 ± 0.6	17.3 ± 0.7
Thrombocyte	PLT	k/µL	862.8 ± 231.5	1025.0 ± 255.0	1001.0 ± 107.0
	MPV	fL	5.6 ± 0.2	5.6 ± 0.1	5.7 ± 0.2

Data represent mean ± SEM for white blood cells (WBC), neutrophils (NE), lymphocytes (LY), monocytes (MO), eosinophils (EO), basophils (BA), red blood cells (RBC), hemoglobin (Hb), hematocrit (HCT), mean corpuscular volume (MCV), mean cell hemoglobin (MCH), mean cell hemoglobin concentration (MCHC), red cell distribution width (RDW), platelets (PLT), and mean platelet volume (MPV). See also Figure 5I in the manuscript.

Table S4. Surface plasmon resonance analysis of AvFc's affinity to viral glycoproteins.

Protein	Virus	Conc. (μg/mL)	K_D (nM)	Chi^2
SF162 (clade B)	HIV	1 – 0.037	0.044 ± 0.007	0.263
E2 (subtype 1b)	HCV	10 – 0.37	5.7 ± 0.8	0.0231
Spike (Beijing02)	SARS-CoV	10 – 0.37	0.53 ± 0.1	0.0126
Spike (EMC 2C/2012)	MERS-CoV	10 – 0.37	0.39 ± 0.04	0.191
Hemagglutinin (New Caledonia)	Influenza A	10 – 0.37	2.2 ± 0.6	0.0564

The binding affinity (K_D) of recombinant proteins to AvFc was measured using a Biacore X100 2.0 instrument at ambient temperature. See **Figure S18**. Data are expressed as mean ± SEM of experimental duplicate analysis.

3. Supplementary Methods

Syncytium formation assay – The assay was performed in triplicate, essentially as previously described, except that HL2/3 cells expressing HIV-1 gp120 were used for fusion with TZM-bl $CD4^+$ target cells[3]. To prepare leaf extract samples, leaf materials were homogenized in 3 v/w extraction buffer (PBS, pH 7.2, 40 mM ascorbic acid) and centrifuged. Samples, diluted 1/20 in GIBCO Dulbecco's modified Eagle's medium (DMEM; Invitrogen) containing 10% fetal bovine serum, 1% penicillin/streptomycin and 500 µg/ml geneticin, were added to 12,000 each of HL2/3 and TZM-bl cells in a 96-well plate, and incubated for 18 h at 37°C in a humid environment containing 5% CO_2. Cells were washed and lysed with 0.05% Triton X-100. To quantify syncytia, a development reagent (60 mM Na_2HPO_4, 40 mM NaH_2PO_4, 10 mM KCl, 1 mM $MgSO_4$, 50 mM 2-mercaptoethanol, 0.8 mg/mL ortho-Nitrophenyl-b-galactoside) was added and incubated at 37°C for 2 to 4 h. The reaction was stopped with 2 M Na_2CO_3, and OD420 was read. Percent syncytium formation was reflected by the reduction in β-galactosidase activity from sample wells versus that of cell only positive control wells.

Surface plasmon resonance (for neonatal Fc receptor [FcRn] binding) – The binding affinity (K_D) of FcRn to AvFc was measured on a Biacore X100 2.0 instrument at ambient temperature. Briefly, $gp120_{CM}$ (NIH AIDS Reagent Program) was immobilized on a CM5 sensor chip (Biacore) to 8,000 resonance units (RUs) using the amine coupling kit (Biacore). A reference flow cell was immobilized with gp120CM to correct response contributions such as bulk shifts that occur equally in the sample and reference flow cells. AvFc was captured on the gp120CM chip to a surface density of about 100-200 RUs. Serial dilutions of recombinant human FcRn (rFCGRT and B2M, Sino Bio# CT009-H08H) (5 µg/ml to 0.0617 µg/ml) were made in running buffer (HPS-EP, GE Healthcare) and injected, at a flow rate of 5 µl/min, for a contact time of 60 s and a dissociation time of 600 s. A blank cycle (running buffer) was performed and all sample injections were blank subtracted to correct the sensorgrams for drifts and other disturbances that affect the reference subtracted curve. Between sample injections the system was washed with running buffer; the immobilized surface was regenerated with Regeneration solution included in the human antibody capture kit. A replicate of a non-zero concentration of FcRn and the blank were injected in each experiment for double referencing, thus verifying the reliability of the immobilized chip throughout the experiment. The data were assessed by Steady State analysis with the Biacore X100 2.0 evaluation software.

Mitogenicity assay – Proliferation of human PBMCs from three different donors was studied by flow cytometry according to well established protocols used in lectin studies[44]. Briefly, cells were treated with AvFc for 72 h and analyzed for any changes in size and/or morphology using forward scatter (FSC) and side scatter (SSC) on a FACSCalibur (BD, San Jose, CA), counting 10,000 events per sample. Data were acquired and analyzed using CellQuest Pro from BD. ConA (10 µg/ml) and PBS were used as controls.

Gene expression analysis in human PBMCs – PBMCs from three blood donors were incubated with AvFc (30 or 100 µg/ml), ConA (10 µg/ml), or buffer vehicle only for 16 h. Cell lysates were homogenized using the Qiagen QIAshredder kit, and a Qiagen RNeasy Mini Kit was used for total RNA extraction and purification. Gene expression was assessed by quantitative RT-PCR using quality verified RNA samples. First strand cDNA was obtained from reverse transcription

of 150 ng RNA using a SUPERSCRIPT VILO cDNA synthesis kit (Life Technologies) according to the manufacturer's instructions. Optimal amounts of template cDNA were added to a reaction mixture containing 10 µl of 2×TaqMan® Fast Advanced Master Mix (Life Technologies) and endonuclease free water to 20 µl and loaded in TaqMan® Array Standard 96 well Plates (Applied Biosystems). These plates contain pre-spotted individual TaqMan® Gene Expression probes for detection of monocyte chemoattractant protein-1 (MCP-1), macrophage inflammatory protein 1α (MIP-1α), Chemokine (C-C motif) ligand 5 also known as Regulated on Activation, Normal T Cell Expressed and Secreted (RANTES), granulocyte-macrophage colony-stimulating factor (GM-CSF), granulocyte colony-stimulating factor (G-CSF), interferon γ–inducible protein-10 (IP-10), interferon gamma-γ (IFN-γ), interleukin (IL)-10, IL-12A, IL-13, IL-15, IL-1A, IL-1B, IL-2, IL-3, IL-4, IL-5, IL-6, IL-7, IL-8, and tumor necrosis factor-α (TNF-α) as well as the house keeping genes 18 S, beta actin (ACTB), and glyceraldehyde 3-phosphate dehydrogenase (GAPDH), summarized in Table S1. PCR amplification was carried out on a 7900HT Fast Real-Time PCR System (Applied Biosystems) in the following conditions: 95°C, 20 min; 40 cycles (95°C, 1 min); 20 min at 60°C. The 7500 software v2.0.6 (Applied Biosystems) was used to determine the cycle threshold (Ct) for each reaction and derive the expression ratios.

Flow cytometric analysis of rhesus macaque PBMCs during AvFc pharmacokinetic analysis – Distribution and activation of rhesus macaque PBMC populations were examined at 0, 4, and 72 h for the two rhesus macaques (RIb15 and RYl15) that received AvFc. Following removal of plasma whole EDTA blood was diluted with PBS and the PBMCs isolated by ficoll gradient centrifugation. Any remain erythrocytes were lysed using an ACK solution. The isolated PBMCs were first labeled for live/dead cells using Alexa fluor 430 (ThermoFisher), followed by surface staining using antibodies to the following markers (clones): CD3 Alexa fluor 700 (SP34-2), CD16 PE-Cy7 (3G8), CD95 FITC (DX2), CD123 PerCP-Cy5.5 (7G3), CD80 PE (L307.4) (all from BD); CD14 Pacific Blue (M5E2), CD8 BV650 (RPA-T8), HLA-DR APC-Cy7 (L243), CD4 BV605(OKT4), CD1c BV711 (L161) (all BioLegend); and CD28 PE- ECD (CD28.2) (Beckman Coulter). Intracellular stain of Ki67 Alexa fluor 647 (b56) was performed using BD Cytofix/Cytoperm™. Samples were acquired on a BD FACSAria Fusion 14-color cytometer and the data analyzed with FlowJo version 10.1r5 (TreeStar, Ashland, OR).